Next-nearest neighbour forces in monatomic superlattices

1991 J. Phys.: Condens. Matter 3 291

(http://iopscience.iop.org/0953-8984/3/3/004)

J. Phys.: Condens. Matter 3 (1991) 291–298. Printed in the UK

Next-nearest neighbour forces in monatomic superlattices

R Hadizad, D R Tilley and J Tilley
Department of Physics, University of Essex, Colchester CO4 3SQ, UK

Received 26 July 1990

Abstract. Results are presented for phonons in a 1D lattice model superlattice. Each frequency ω corresponds to two Bloch wavenumbers Q_1 and Q_2. For $\alpha > 0.25$, where α is the ratio of next-nearest to nearest forces, both wavenumbers can be real over some frequency range. Dispersion curves are given and discussed for various values of α and of the mass ratio m_2/m_1 between the components of the superlattice.

1. Introduction

The lattice dynamics of superlattices has been the subject of intensive study, both theoretical and experimental, for the last ten years; a useful review is given by Sapriel and Djafari-Rouhani (1989). Considerable insight is gained from the study of simple 1D systems, both monatomic and diatomic, with nearest-neighbour forces. A 1D superlattice consisting of n_1 atoms of component 1 followed by n_2 atoms of component 2, repeated periodically, has a long period $L = (n_1 + n_2)a$, where a is the atomic spacing, assumed the same in both components. In consequence a 'mini Brillouin zone' with a boundary at $\pi/L = (n_1 + n_2)^{-1}\pi/a$ appears. In a reduced-zone scheme, the acoustic and optic phonon branches appear folded in the mini Brillouin zone, with gaps related to the long period appearing at the zone edges. The higher-order folded acoustic phonon modes occur at sufficiently high frequency to be detected by Raman scattering, and indeed the appearance of folded-phonon doublets is a characteristic feature of the Raman spectra of good-quality superlattices. Similarly, optic-phonon doublets are seen. Thus 1D models have considerable value in their own right. Furthermore, the dispersion curves found from a calculation based on 3D lattice dynamics can often be replicated by those derived from a 1D model with appropriate effective interactions (Molinari 1991).

We present here a detailed study of the effect of including next-nearest neighbour (NNN) forces in a 1D monatomic superlattice. Although some of the effective-interaction 1D models include next (and indeed further) interactions, their presence has been seen only as leading to a modification of the nearest-neighbour (NN) dispersion curves. As we shall see, however, when the ratio $\alpha = C_2/C_1$ of next-nearest to nearest neighbour forces is sufficiently large (specifically when $\alpha > 0.25$) qualitatively different effects arise.

We start, in section 2, by reviewing the lattice dynamics of a bulk 1D crystal including NNN forces. The main difference from the NN case is that for every frequency ω there are four allowed values of wavenumber q, say $\pm q_1$, $\pm q_2$, rather than the two values $\pm q_1$

0953-8984/91/030291 + 08 $03.50

found with NN forces only. For low frequency $\omega a/v \ll 1$, where v is the acoustic-phonon velocity, q_1 is real while q_2 is complex and of the form $\pi/a + iy$, with y large. However, for $\alpha > 0.25$ there is a higher frequency interval in which both q_1 and q_2 are real, and it is in this interval that the most interesting new effects arise in the superlattice dispersion curves.

Section 3.1 contains the formal results for the superlattice. Within each component of the superlatice the atomic displacements may be written as a coherent superposition of the four waves $\exp(\pm q_1 x)$, $\exp(\pm q_2 x)$. This superposition is given by the 4D vector $(abcd)^{\mathsf{T}}$, where a, b, c and d are the amplitudes of the four waves. The dynamics of the superlattice are contained in the transfer matrix $\mathbf{T}$, which relates the amplitudes in the cell starting at $(\ell + 1)L$, say, to those in the cell starting at ℓL. Clearly $\mathbf{T}$ is 4×4. It is derived as a product of matrices $\mathbf{F}$ describing transfer of amplitudes across one component and matrices $\mathbf{M}$ describing transfer across an interface. The latter are found from the equations of motion of four atoms, two on each side of the interface. As in the NN lattice, for which $\mathbf{T}$ is 2×2, $\mathbf{T}$ is unimodular, $\det \mathbf{T} = 1$, so that the eigenvalues satisfy $\lambda_1\lambda_2\lambda_3\lambda_4 = 1$. In addition, since time-reversal invariance applies, the eigenvalues occur in two pairs $(\lambda_1, \lambda_1^{-1})$ and $(\lambda_2, \lambda_2^{-1})$. Bloch vectors Q_n are related to the eigenvalues by $\exp(iQ_nL) = \lambda_n$. Therefore, just as there are two wavenumbers q_1 and q_2 in the bulk material, there are two Bloch wavenumbers in the superlattice. Depending on the frequency, neither, one or both may be real.

The formal results of section 3.1 are illustrated in section 3.2 with graphs of various dispersion curves. Some discussion of the results and their implications is given in section 4.

2. Bulk crystal

We consider the model shown schematically in figure 1(*a*). The equation of motion for the displacement u_n of mass n is

$$-m\omega^2 u_n = C_1(u_{n+1} + u_{n-1} - 2u_n) + C_2(u_{n+2} + u_{n-2} - 2u_n). \tag{1}$$

The infinite series of equations represented by (1) is solved by the ansatz

$$u_n = \exp(inqa) \tag{2}$$

provided

$$m\omega^2 = 2C_1(1 - \cos qa) + 2C_2(1 - \cos 2qa) \tag{3}$$

which is conveniently written as an equation for $\cos\eta$ where $\eta = qa$:

$$2\alpha\cos^2\eta + \cos\eta + (\Omega^2 - 1 - 2\alpha) = 0 \tag{4}$$

where

$$\Omega^2 = m\omega^2/2C_1 \tag{5}$$

$$\alpha = C_2/C_1 \tag{6}$$

Equation (4) has two solutions for $\cos\eta$, and therefore as stated in section 1 equation (3) has four solutions for q, say $\pm q_1$ and $\pm q_2$. It is easily seen that for small Ω, only one value of η is real, and the other takes the form $\pi + iy$ since $\cos\eta < -1$. For $\alpha < 0.25$,

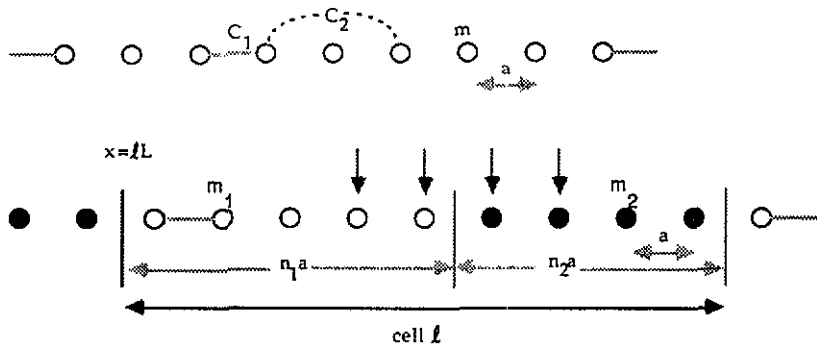

Figure 1 (*a*). Bulk 1D next-nearest neighbour (NNN) crystal, with notation defined. (*b*) Superlattice model for section 3. Spring constants are the same throughout as in (*a*).

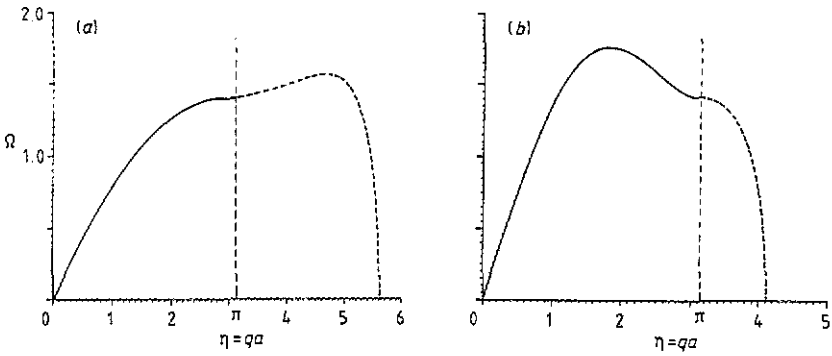

Figure 2. Bulk dispersion curves, Ω versus $\eta = qa$ for (*a*) $\alpha = 0.1$ and (*b*) $\alpha = 1.0$. The convention for η of the form $\pi + iy$ is that these values are represented as broken curves with y as the abscissa measured from $\eta = \pi$. Dimensionless frequency Ω is defined in (5).

there is no frequency interval in which both values of η are real. For $\alpha > 0.25$, however, both values of η are real in the frequency interval

$$2 < \Omega^2 < 1 + 2\alpha + 1/8\alpha. \tag{7}$$

Solutions of (4) are illustrated in figure 2 for two values of α. For $\alpha = 0.1$ the real-q curve is very similar to that found for NN forces, as might be expected, and the complex-q curve corresponds to such large y values that its effect on superlattice properties is negligible. For $\alpha = 1.0$, on the other hand, both q values are real over the range (7), and even for $\Omega^2 < 2$ the y value is fairly small. It will be seen that significant changes from the NN superlattice dispersion curves arise for such large values of α.

3. Superlattices

3.1. Formalism

The model to be considered is defined in figure 1(*b*). The spring constants are taken to be the same throughout, with values as shown in figure 1(*a*), so that the two components

of the superlattice differ only in their mass values. The equations of motion for an atom within component 1 of cell ℓ are satisfied by a superposition of waves involving $\pm q_{11}$, $\pm q_{12}$, where q_{11} and q_{12} are the solutions of equation (3) with mass m_1. This superposition can be written in two forms:

$$u = a^{\mathrm{L}} \exp[\mathrm{i}q_{11}(x - \ell L)] + b^{\mathrm{L}} \exp[-\mathrm{i}q_{11}(x - \ell L)] + c^{\mathrm{L}} \exp[\mathrm{i}q_{12}(x - \ell L) + d^{\mathrm{L}} \exp[-\mathrm{i}q_{12}(x - \ell L)] \tag{8}$$

or

$$u = a^{\mathrm{R}} \exp[\mathrm{i}q_{11}(x - \ell L - n_1 a)] + b^{\mathrm{R}} \exp[-\mathrm{i}q_{11}(x - \ell L - n_1 a)] + c^{\mathrm{R}} \exp[\mathrm{i}q_{12}(x - \ell L - n_1 a)] + d^{\mathrm{R}} \exp[-\mathrm{i}q_{12}(x - \ell L - n_1 a)]. \tag{9}$$

The displacements are described by either of the vectors $|U^{\mathrm{L}}\rangle = (a^{\mathrm{L}} b^{\mathrm{L}} c^{\mathrm{L}} d^{\mathrm{L}})^{\mathrm{T}}$ or $|U^{\mathrm{R}}\rangle = (a^{\mathrm{R}} b^{\mathrm{R}} c^{\mathrm{R}} d^{\mathrm{R}})^{\mathrm{T}}$ which are related by

$$|U^{\mathrm{R}}\rangle = \mathbf{F}_1 |U^{\mathrm{L}}\rangle \tag{10}$$

where $\mathbf{F}_1$ is the diagonal matrix $[f_{11}\bar{f}_{11}f_{12}\bar{f}_{12}]$ with

$$f_{ij} = \exp(\mathrm{i}q_{ij}d_j) \qquad \bar{f}_{ij} = \exp(-\mathrm{i}q_{ij}d_j) \qquad i, j = 1, 2 \tag{11}$$

$$d_j = n_j a. \tag{12}$$

The displacements in component 2 are described similarly by vectors $|W^{\mathrm{L}}\rangle = (e^{\mathrm{L}} f^{\mathrm{L}} g^{\mathrm{L}} h^{\mathrm{L}})^{\mathrm{T}}$ or $|W^{\mathrm{R}}\rangle = (e^{\mathrm{R}} f^{\mathrm{R}} g^{\mathrm{R}} h^{\mathrm{R}})^{\mathrm{T}}$, related by a phase matrix $\mathbf{F}_2$.

The equations of motion of the four atoms at the interface, marked in figure 1(*b*), relate $|W^{\mathrm{L}}\rangle$ to $|U^{\mathrm{R}}\rangle$. The result is

$$\mathbf{M}_1 |U^{\mathrm{R}}\rangle = \mathbf{M}_2 |W^{\mathrm{L}}\rangle \tag{13}$$

and likewise at the next interface to the right

$$\mathbf{M}_2 |W^{\mathrm{R}}\rangle = \mathbf{M}_1 |U^{\mathrm{L}}_{\ell+1}\rangle \tag{14}$$

where subscript $\ell + 1$ indicates the next superlattice cell and

$$\mathbf{M}_i = \begin{pmatrix} 1 & 1 & 1 & 1 \\ \bar{s}_{i1} & s_{i1} & \bar{s}_{i2} & s_{i2} \\ s_{i1}^2 & \bar{s}_{i1}^2 & s_{i2}^2 & \bar{s}_{i2}^2 \\ s_{i1} & \bar{s}_{i1} & s_{i2} & \bar{s}_{i2} \end{pmatrix} \qquad i = 1, 2 \tag{15}$$

where

$$s_{ij} = \exp(\mathrm{i}q_{ij}a) \qquad \bar{s}_{ij} = \exp(-\mathrm{i}q_{ij}a) \tag{16}$$

The transfer matrix $\mathbf{T}$ is defined by

$$|U^{\mathrm{L}}_{\ell+1}\rangle = \mathbf{T}|U^{\mathrm{L}}_{\ell}\rangle = \mathbf{M}_1^{-1}\mathbf{M}_2\mathbf{F}_2\mathbf{M}_2^{-1}\mathbf{M}_1\mathbf{F}_1|U^{\mathrm{L}}_{\ell}\rangle. \tag{17}$$

The determinant $\det \mathbf{T}$ is the product of the determinants of the matrices shown explicitly in (17); since $\det \mathbf{F}_i = 1$

$$\det \mathbf{T} = 1. \tag{18}$$

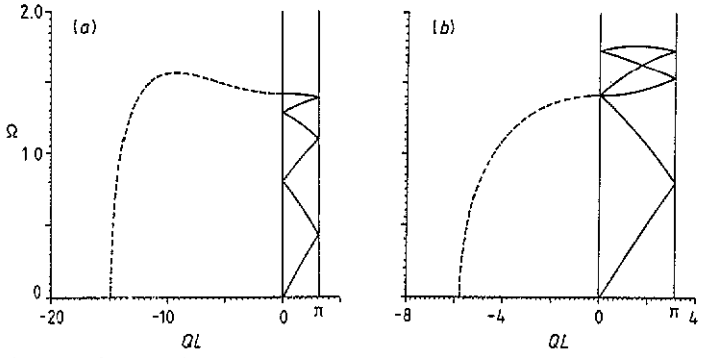

Figure 3. Superlattice dispersion curves for $n_1 = n_2 = 3$ for identical components, $m_1 = m_2$ (*a*) $\alpha = 0.1$ and (*b*) $\alpha = 1.0$. The convention for complex QL of the form iy is that these values are represented as broken curves with y as the negative of the abscissa measured from $QL = 0$.

as usual for simple 2×2 transfer matrices. Hence the eigenvalues λ_1 to λ_4 of **T** satisfy

$$\lambda_1\lambda_2\lambda_3\lambda_4 = 1. \tag{19}$$

Bloch's theorem states that solutions of the dynamical equations can be found that transform according to the irreducible representations of the translation operator for the superlattice period, viz

$$|U_{\ell+1}^{L}\rangle = \exp(\mathrm{i}QL)|U_{\ell}^{L}\rangle \tag{20}$$

Q need not be real, but time-reversal invariance requires that if Q is a root, so is $-Q$. Comparison of (17) and (20) shows that $\exp(\mathrm{i}QL)$ is one of the eigenvalues of **T**, so we conclude that, as mentioned in section 1, the eigenvalues occur in pairs $(\lambda_1, \lambda_1^{-1})$ and $(\lambda_2, \lambda_2^{-1})$, which are related to the two Bloch wavenumbers Q_i by

$$\exp(\mathrm{i}Q_iL) = \lambda_i \qquad i = 1, 2 \tag{21}$$

In the NN case, it is usually possible to find an explicit expression for the 2×2 transfer matrix, so that an explicit dispersion relation can be derived from (22); several examples are reviewed by Cottam and Tilley (1989). We have used a symbolic algebra package (Macsyma) to find the analytic forms of the elements of **T** for the NNN case; the expressions are given elsewhere (Hadizad 1991). However, the analytic form of the dispersion equation is very cumbersome, and it is easier to calculate graphs direct from the matrix equations presented in this section and the previous section.

3.2. Numerical results

In this section we illustrate the results of section 3.1, with a variety of dispersion curves. We follow convention by presenting these as frequency ω versus wavenumber Q. However, the numerical work is very much easier if ω is regarded as the independent variable, so that the two Bloch wavenumbers Q are evaluated for each value of ω. The procedure is as follows. For a given parameter α, and for each ω, the four bulk wavenumbers q_{ij} are evaluated from (4). This enables determination of the interface

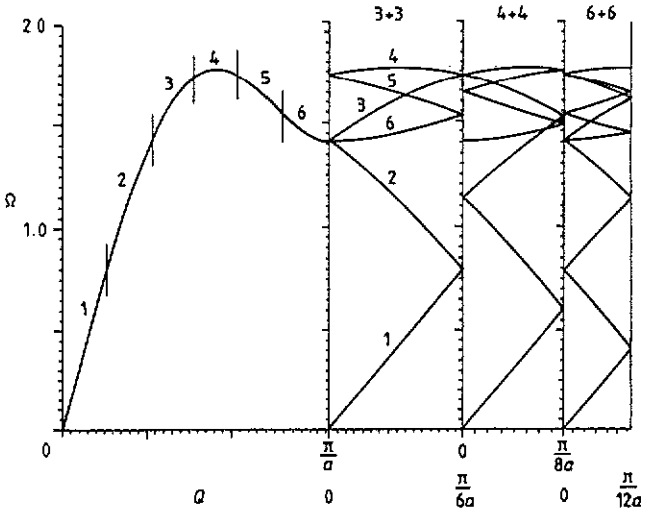

Figure 4. Real parts of dispersion curves for 3 + 3, 4 + 4 and 6 + 6 superlattices with $\alpha = 1$ and identical components, $m_1 = m_2$. The real part of the $\alpha = 1$ bulk dispersion curve is also shown, with the 3 + 3 folding indicated. The horizontal scale for the bulk graph is compressed by a factor 3.

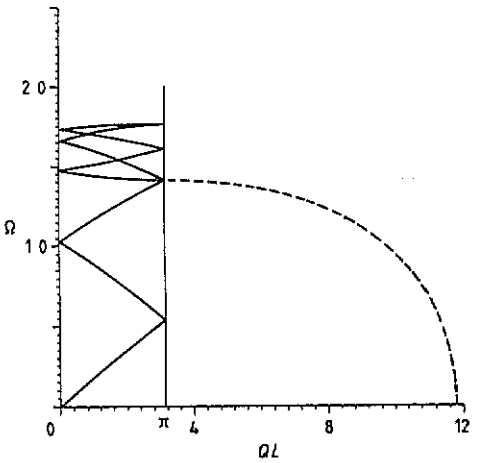

Figure 5. Dispersion curve for a 3 + 6 superlattice with $m_1 = m_2$ and $\alpha = 1.0$.

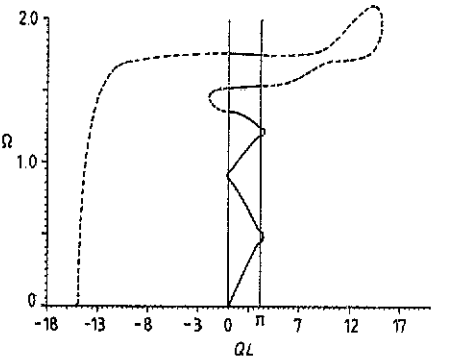

Figure 6. Dispersion curve for a 3 + 3 superlattice with $\alpha = 0.1$ and $m_2/m_1 = 0.6$.

matrices $\mathbf{M}_i$, defined in (15), then given values of n_1 and n_2 the phase matrices can be found from (10). $\mathbf{T}$ is then evaluated from (18), and the eigenvalues are found in a standard way. Finally the Bloch wavenumbers are given by (22).

It is helpful to start with the dispersion curves for the case when the two superlattice components have identical masses, $m_1 = m_2$. This is the equivalent of the free-electron model in electron-band theory, so that the bulk dispersion curve is folded into the mini Brillouin zone without any stop bands appearing. This is illustrated for the 3 + 3 superlattice for $\alpha = 0.1$ and $\alpha = 1$ in figure 3, which shows the folding of the real-q curve

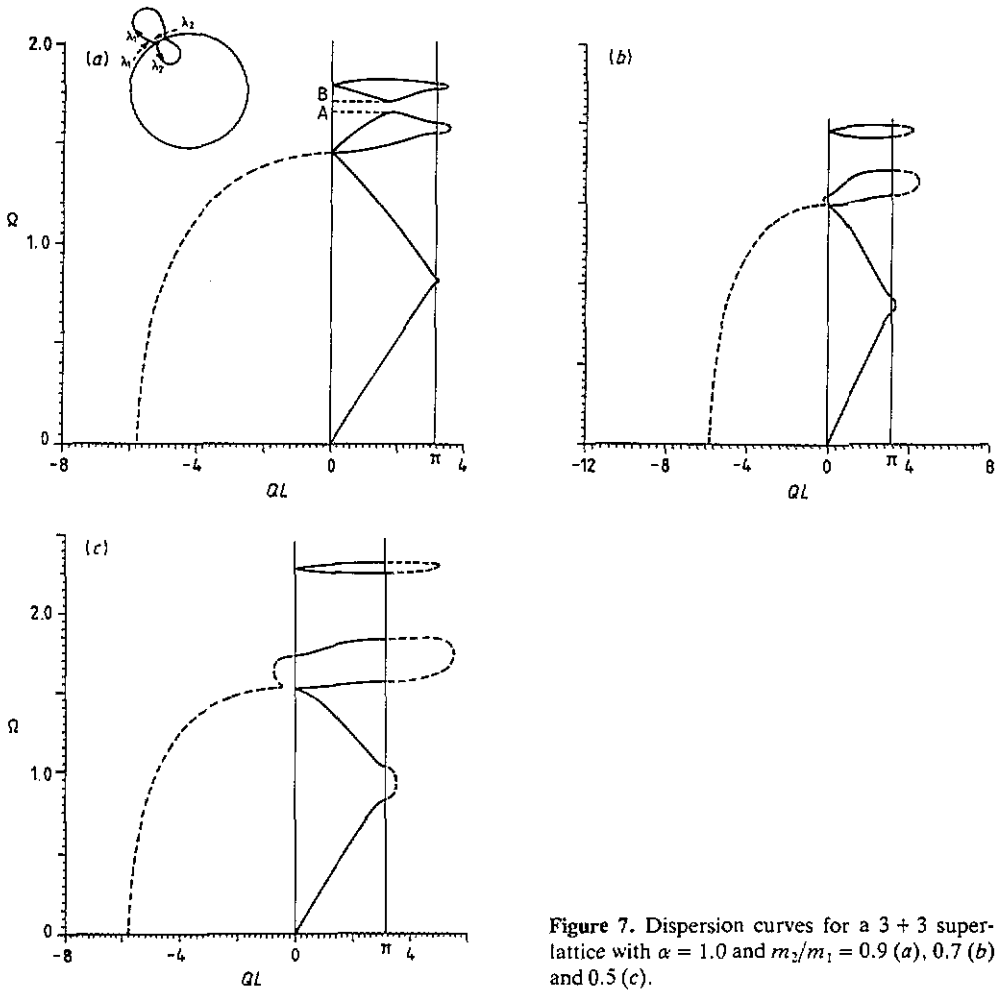

Figure 7. Dispersion curves for a 3 + 3 superlattice with $\alpha = 1.0$ and $m_2/m_1 = 0.9$ (*a*), 0.7 (*b*) and 0.5 (*c*).

of figure 2. In addition, the complex root of the form $\pi + iy$ is 'folded' to the form iy. The folding is further illustrated in figure 4, which shows the real-Q curves for the 4 + 4 and 6 + 6 superlattices in addition to the 3 + 3 superlattice for $\alpha = 1$. We show in parallel the real-q bulk dispersion curve for $\alpha = 1$, with an indication of how the different parts are folded to give the 3 + 3 curves. The fact that the complex root $\pi + iy$ folds to iy for the 3 + 3 superlattice is simply a consequence of the fact that there is an even number of atoms in the superlattice unit cell; for an odd number the folding is to $\pi + iy$, as illustrated in figure 5 for the 3 + 6 superlattice with $m_1 = m_2$.

For $m_1 \neq m_2$ stop bands appear in the dispersion curve. When the NNN force is weak, the modification of the real-Q branches is very similar to what is known for the NN case, and as with $m_1 = m_2$ the complex roots remain well away from the real axis. An example is shown in figure 6.

The effect of varying the mass ratio for a larger value of α is illustrated in figure 7. The curves there are clearly related to that shown in figure 3 by the introduction of stop bands both at the zone edges and also at crossing points between different branches.

Equation (21) may be used to express the behaviour of the Bloch wave vector Q in the various stop bands in terms of the underlying eigenvalue λ of the transfer matrix **T**. Real Q corresponds to eigenvalues λ and λ^{-1} on the unit circle. An excursion $QL = \pi + iy$, represented on a graph to the right of the mini Brillouin zone, corresponds to an excursion of λ off the unit circle along the negative real axis from $\lambda = \lambda^{-1} = -1$, say $\lambda < -1$ and $-1 < \lambda^{-1} < 0$. Similarly $QL = iy$, represented as a graph to the left of the mini Brillouin zone, corresponds to an excursion of λ along the positive real axis, $\lambda > 1$ and $0 < \lambda^{-1} < 1$. Within a stop band like AB in figure 7(*a*) there are still four eigenvalues $\lambda_1, \lambda_1^{-1}, \lambda_2, \lambda_2^{-1}$ of **T**. λ_1 and λ_2 coincide at A, then undergo excursions off the unit circle as sketched in the insert to figure 7(*a*). Comparison of figures 7(*a*), 7(*b*) and 7(*c*) shows that, as might be expected, the frequency widths of the stop bands increase as m_2/m_1 deviates further from unity. Over most of the frequency range $\Omega < 1.7$, however, the pure imaginary root $QL = iy$ is more or less independent of the value of m_2/m_1.

4. Discussion

As might be expected, the introduction of weak NNN interactions produces only small perturbations to the well-known results for the NN case. In principle a second Bloch wavevector Q appears, but it is seen from figures 3(*a*) and (*b*) that it is typically quite far off the real axis. A Q having such a large imaginary part corresponds to displacements that decay rapidly with distance from an interface, and therefore has little physical significance. For stronger interactions, $\alpha = C_2/C_1 > 0.25$, however, the bulk dispersion curve has a maximum within the Brillouin zone, and therefore there is a range of frequencies for which the phonon dispersion curve has two real values of q for a given ω. This is illustrated in figure 2(*b*). In consequence the folding induced by the superlattice period, as in figures 3(*b*), and 4, produces a more involved spectrum, with two real Bloch vectors Q appearing over an extended frequency range. As the mass ratio m_2/m_1 deviates from unity, stop bands appear in the superlattice dispersion curve. In addition to the stop bands at $QL = 0$ and π, familiar from the NN case, stop bands can also appear at an interior point of the mini Brillouin zone, like the band AB in figure 7(*a*). Surface modes, in which the vibration amplitude decays with distance from the surface of a semi-infinite superlattice, may be expected to appear within the stop bands.

We have concentrated on the formal differences due to the introduction of NNN interactions, in particular the appearance of a second Bloch wavenumber and the more complicated mode patterns that arise for $\alpha > 0.25$. It is to be hoped that these forms of folded acoustic modes might be studied by Raman scattering.

The present calculations can be extended to diatomic superlattices, where the presence of the optic-phonon bands leads to considerable complications. We hope to present results for this case shortly.

References

Cottam M G and Tilley D R 1989 *Introduction to Surface and Superlattice Excitations* (Cambridge: Cambridge University Press) ch 7

Hadizad R 1991 *PhD thesis* University of Essex

Molinari E 1991 *Light Scattering from Semiconductor Structures and Superlattices* ed D J Lockwood and J F Young (New York: Plenum) at press

Sapriel J and Djafari Rouhani B 1989 *Surf. Sci. Rep.* **10** 189